Accepted Manuscript

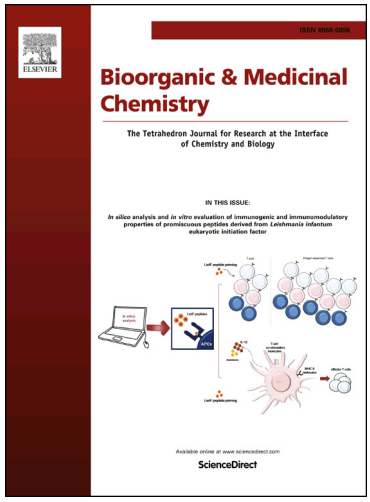

Discovery of New Thienopyrimidine Derivatives as Potent and Orally Efficacious Phosphoinositide 3-Kinase Inhibitors

Songwen Lin, Chunyang Wang, Ming Ji, Deyu Wu, Yuanhao Lv, Li Sheng, Fangbin Han, Yi Dong, Kehui Zhang, Yakun Yang, Yan Li, Xiaoguang Chen, Heng Xu

PII: S0968-0896(17)32142-9
DOI: https://doi.org/10.1016/j.bmc.2017.12.025
Reference: BMC 14130

To appear in: *Bioorganic & Medicinal Chemistry*

Received Date: 4 November 2017
Revised Date: 17 December 2017
Accepted Date: 19 December 2017

Please cite this article as: Lin, S., Wang, C., Ji, M., Wu, D., Lv, Y., Sheng, L., Han, F., Dong, Y., Zhang, K., Yang, Y., Li, Y., Chen, X., Xu, H., Discovery of New Thienopyrimidine Derivatives as Potent and Orally Efficacious Phosphoinositide 3-Kinase Inhibitors, *Bioorganic & Medicinal Chemistry* (2017), doi: https://doi.org/10.1016/j.bmc.2017.12.025

Bioorganic & Medicinal Chemistry
journal homepage: www.elsevier.com

Discovery of New Thienopyrimidine Derivatives as Potent and Orally Efficacious Phosphoinositide 3-Kinase Inhibitors

Songwen Lin [a,1], Chunyang Wang [a,1], Ming Ji [a], Deyu Wu [b], Yuanhao Lv [a], Li Sheng [c], Fangbin Han [d], Yi Dong [b], Kehui Zhang [b], Yakun Yang [c], Yan Li [c], Xiaoguang Chen [a,*], Heng Xu [a,*]

[a] *State Key Laboratory of Bioactive Substance and Function of Natural Medicines, Institute of Materia Medica, Chinese Academy of Medical Sciences and Peking Union Medical College, Beijing 100050, China.*
[b] *Beijing Key Laboratory of Active Substances Discovery and Drugability Evaluation, Institute of Materia Medica, Chinese Academy of Medical Sciences and Peking Union Medical College, Beijing 100050, China.*
[c] *Beijing Key Laboratory of Non-Clinical Drug Metabolism and PK/PD study, Chinese Academy of Medical Sciences and Peking Union Medical College, Beijing 100050, China*
[d] *PKUCare Pharmaceutical R&D Center, Beijing 102206, China*

ARTICLE INFO

Article history:
Received
Received in revised form
Accepted
Available online

Keywords:
Phosphoinositide 3-kinase inhibitors
anti-tumor activities
thienopyrimidine
acetylation

ABSTRACT

A series of new thienopyrimidine derivatives has been discovered as potent PI3K inhibitors. The systematic SAR studies for these analogues are described. Among them, **8a** and **9a** exhibit nanomolar enzymatic potencies and sub-micromolar cellular anti-proliferative activities. **8a** displays favorable pharmacokinetic profiles, while **9a** easily undergoes deacetylation to yield a major metabolite **8a**. Furthermore, **8a** and **9a** potently inhibit tumor growth in a dose-dependent manner in the NCI-H460 xenograft model with an acceptable safety profile.

1. Introduction

Phosphoinositide 3-kinases (PI3Ks) are a family of lipid kinases that are involved in many essential cellular functions including cell growth, proliferation, differentiation, motility, survival, and intracellular trafficking.[1-3] Depending upon their sequence homology and substrate preferences, PI3Ks are divided into three distinct classes (I, II & III).[3] The class I PI3Ks are most intensively studied to date and consist of a regulatory subunit and a catalytic subunit. The catalytic subunit occurs in four isoforms designated as p110α, p110β, p110γ and p110δ. Signaling from receptor tyrosine kinases and G-protein-coupled receptors, the class I PI3Ks catalyze the phosphorylation of the 3'-hydroxyl group of phosphatidylinositol 4,5-biphosphate (PIP2) to generate phosphatidylinositol 3,4,5-triphosphate (PIP3). PIP3 functions as a potent secondary cellular messenger to initiate a signal transduction cascade leading to activation of the serine/threonine kinase AKT (also known as protein kinase B or PKB).[3] The activated AKT in turn triggers the downstream signaling events that ultimately stimulates mammalian target of rapamycin (mTOR) that plays a key role in regulating cell growth, survival and proliferation.[4] Moreover, phosphatase and tensin homologue (PTEN), a lipid phosphatase that catalyzes the dephosphorylation of PIP3, is identified as a major negative regulator of the PI3K pathway.[5]

The PI3K pathway is one of the most frequently aberrantly activated signaling pathways in human cancers.[3, 6] Molecular alterations in this pathway are significantly associated with tumorigenesis.[7] According to a recent analysis on 19,784 consecutive tumor samples (> 40 cancer types), 38% of patients had at least one alternation in the PI3K pathway components.[8] Inhibition of this pathway therefore provides a promising approach to discover novel therapeutics for cancer treatment. A number of dual PI3K/mTOR, pan-PI3K and isoform selective PI3K inhibitors have entered into clinical trials, alone or in combination, in both solid tumors and hematologic malignancies.[9-12] In 2014, FDA approved the first-in-class PI3Kδ inhibitor Idelalisib for the treatment of patients with three types of hematologic cancers (CLL, FL and SLL).[13] In 2017, the class I PI3K inhibitor copanlisib received an accelerated approval from FDA for the treatment of relapsed follicular lymphoma based on a single-arm trial that included only 104 patients (Figure 1).[14]

* Corresponding author. *Email addresses*: chxg@imm.ac.cn; xuheng@imm.ac.cn

[1] These authors contributed equally to this work.

Copanlisib showed preferential activity against PI3Kα and p110δ as compared with PI3Kβ and p110γ.[15] Extensive efforts to develop PI3K inhibitors to treat solid tumors are still ongoing. However, emerging clinical data showed those PI3K inhibitors had limited single-agent activities in solid tumors and none has yet reached a regulatory approval.[16] Clearly, challenges remain for PI3K inhibitors to become a significant component of the anticancer portfolio. To address these challenges, future directions for clinical development of PI3K inhibitors are getting a greater focus on patient selection, rational combination as well as understanding of immune modulation.[16-18] From medicinal chemistry point of view, identification of more structurally diversified PI3K inhibitors would provide opportunities to differ their pharmacological and safety profiles, thereby facilitating discovery of inhibitors targeting PI3K pathway with better clinical outcomes.

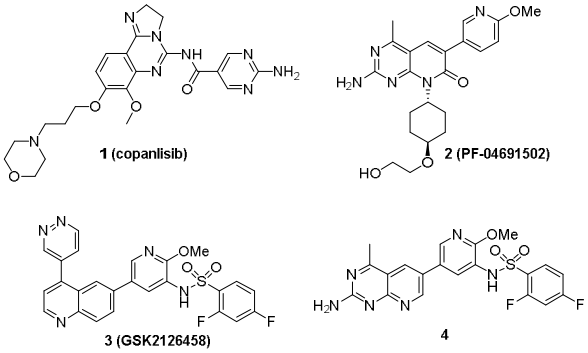

Fig. 1. Selected PI3K inhibitors (**1** - **4**).

As previously reported, we disclosed a series of 2-amino-4-methylpyrido[2,3-*d*]pyrimidine derivatives as potent PI3K inhibitors, in which the key aminopyridopyrimidine, sulfonamide and pyridyl nitrogen moieties interacts with Val 882, Lys 833, and a conserved water molecule respectively in the ATP binding pocket.[19] Among them, the representative compound **4** provided potent inhibition of PI3Kα with an IC_{50} of 2.0 nM and a reasonable U87 cell IC_{50} of 0.63 μM (Fig. 1). However, **4** could not achieve tumor growth inhibition in in vivo xenograft models at various doses, probably due to its undesirable ADME properties originated from poor physicochemical properties. In this paper, we explored various 6,6- and 6,5- bicycles (**5**-**9**) as alternatives to the pyridopyrimidine core in the previous scaffold and further optimization led to the discovery of a series of new thienopyrimidine derivatives (**8a** and **9a**) that demonstrated excellent enzymatic, cellular and *in vivo* antitumor activities.

2. Results and discussion

2.1. Chemistry

The representative synthetic approach for thienopyrimidine derivatives **8a-h** and **9a-g** was described in Scheme 1. The starting material **10** was prepared according to the reported methods.[20] Treatment of **10** with methylboronic acid afforded **11**, which was brominated with NBS and then deprotected to afford the key intermediate **13**. **13** was then converted to **14a-e** by either acylation or methylation. Finally, **13** and **14a-e** were coupled with various aryl boronic esters to yield target compounds **8a-h** and **9a-g**.

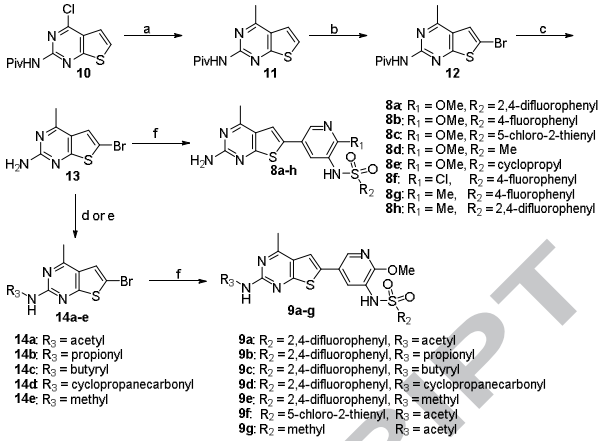

Scheme 1. Synthesis of compounds **8a-h** and **9a-g**. Reagents and conditions. (a) methylboronic acid, 2M K_2CO_3, $PdCl_2$(dppf), 1,4-dioxane, 105 °C, 3 h, Ar, 42%; (b) NBS, DMF, rt, 4 h, 76%; (c) 2M NaOH, EtOH, 90 °C, 1.5 h, 82%; (d) acyl chloride, pyridine, DMF, rt, 4 h, 52-60%; (e) MeI, NaH, DMF, rt, 4 h, 28%; (f) aryl boronic ester, $PdCl_2$(dppf), 2M K_2CO_3, dioxane, 100 °C, Ar, 4-6 h, 20-59%.

2.2. Enzymatic and cellular assays

Table 1. SAR of pyridopyrimidine replacements.

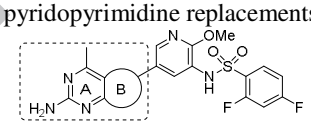

Compd.	bicycles	PI3K IC50 (nM)[a]	U87MG IC50 (μM)[b]
4	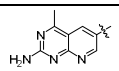	2.0	0.63
5	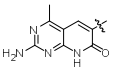	6.1	>50
6	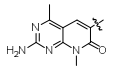	2.4	0.96
7	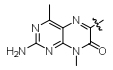	1.3	0.63
8a	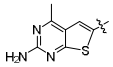	1.3	2.4
PI-103	--	7.4	--
PF-04691502	--	--	0.34

[a] The IC_{50}s are mean values of duplicates.
[b] The IC_{50}s are mean values of triplicates.

Our initial structural modification focused on replacement of the pyridopyrimidine core of compound **4** with different 6,6- and 6,5- bicycles as these bicycles were envisioned to adopt similar binding topologies that could maintain major interactions with the PI3K kinase (Table 1). Pyridopyrimidinone **5** and **6** were firstly synthesized for evaluation. As shown in Table 1, both compounds displayed effective kinase inhibition with single-digit nanomolar potencies against PI3Kα, comparable to **4**. Notably, compound **5** was inactive in a U87 cellular assay (IC_{50} > 50 μM). We reasoned that the NH proton of the pyridopyrimidinone in **5** deleteriously affected its membrane permeability. Pteridin-7(8*H*)-one **7** demonstrated similar PI3Kα and cellular potencies relative to **4** and **6**, indicating 6,6-bicylics was generally a good scaffold to project the key peripheral moieties to access the key interactions. It is important to note that the 6,5-bicyclic thienopyrimidine **8a**, structurally distinct from above 6,6-

bicycles, potently inhibit PI3Kα kinase with an IC_{50} of 1.3 nM, while its U87 cellular proliferation activity was considerably lower than those of pyridopyrimidinone **6** and pteridin-7(8*H*)-one **7**. Encouraged by its differentiated structure bearing nanomolar PI3Kα potency, thienopyrimidine **8a** was further derivatized to improve its cellular activity along with other drug-like properties.

Sulfonamide functionality in **8a** was subsequently targeted to modify given that the deprotonated sulfonamide NH at physiological conditions could form charge interactions with Lys833 to increase the potency (Table 2).[21, 22] 4-fluorobenzene-sulfonamide **8b** exhibited the similar level of both PI3K and U87 cellular potencies in comparison to **8a**. When 5-chlorothiophene was introduced, U87 cellular potency dropped ~3 fold while PI3Kα potency maintained (**8c** vs **8a**). Methanesulfonamide **8d** and cyclopropanesulfonamide **8e** displayed decreased potencies for both PI3Kα and U87 cellular growth inhibition relative to **8a**. To explore the SAR, methoxy group adjacent to the pyridine nitrogen was changed to other small substituents (e.g. Cl or Me) and the corresponding **8f**, **8g** and **8h** showed a significant decrease in cellular activity (~2-6 fold decrease relative to **8a**). Overall, above variations on sulfonamide functionality failed to yield compounds with improved cellular potencies.

Table 2. SAR of pyridine substituents.

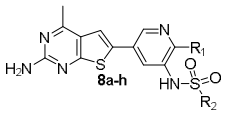

Compd.	R_1	R_2	PI3Kα IC_{50} (nM)[a]	U87MG IC_{50} (μM)[b]
8a	OMe		1.3	2.4
8b	OMe		2.2	2.9
8c	OMe		1.5	8.1
8d	OMe	CH_3-	2.8	3.0
8e	OMe		5.6	6.5
8f	Cl		2.2	5.8
8g	Me		9.3	15
8h	Me		3.0	8.7
PI-103	--	--	7.4	--
PF-04691502	--	--	--	0.34

[a] The IC_{50}s are mean values of duplicates.

[b] The IC_{50}s are mean values of triplicates.

The challenge of translating its enzymatic inhibition into potent cellular activity for these thienopyrimidine derivatives still remains to be tackled. Finally, we turned our attention to the polar pyrimidylamino group. To mask the amino group, we carried out various amidation as well as methylation reactions. As shown in Table 3, in comparison to their free amine form **8a**, acetamide **9a**, propionamide **9b** and butyramide **9c** more or less maintained its enzymatic potency. More importantly, the amidation can give rise to enhanced cellular potency (**9a** and **9b** vs **8a**, respectively). In particular, acetamide **9a** had an IC_{50} of 0.3 μM in a U87 cell proliferation assay, around 8 fold improvement over that of **8a**. This improvement was mainly attributed to its enhanced permeability as observed in a PAMPA assay (Table 4, **8a** vs **9a**, 4.8×10^{-6} cm/s vs 9.6×10^{-6} cm/s). It is also worth noting that methylation of **8a** yielded less potent compound **9e** compared to acetylation. Further structural modification was to vary sulfonamide functionality while retaining the acetamide moiety. It was found that acetylation could also boost cellular potency for 5-chlorothiophene-2-sulfonamide (**8c** vs **9f**), but, in contrast, it could not make improvement on methanesulfonamide (**8d** vs **9g**).

Table 3. SAR of the pyrimidine amine and sulphonamide.

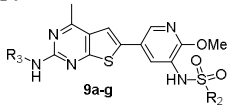

Compd.	R_2	R_3	PI3Kα IC_{50} (nM)[a]	U87MG IC_{50} (μM)[b]
9a			1.1	0.30
9b			2.2	1.5
9c			1.6	2.3
9d			2.3	6.5
9e		CH_3	1.6	2.1
9f			1.0	0.70
9g	CH_3		4.5	3.0
PI-103	--	--	7.4	--
PF-04691502	--	--	--	0.34

[a] The IC_{50}s are mean values of duplicates.

[b] The IC_{50}s are mean values of triplicates.

*2.3. In vitro profile of **8a** and **9a***

On the basis of the above SAR exploration, **8a** and its acetylated counterpart **9a** were then selected for further profiling (Table 4). **8a** and **9a** potently inhibited all four different class I PI3K isoforms (α, β, δ and γ). While they are least potent against PI3Kγ with an IC_{50} of ~10 nM, **8a** and **9a** did not show an appreciated selectivity for those isoforms. As anticipated, **8a** and **9a** also had mTOR inhibitory activity since it shares a high degree of sequence homology with class I PI3Ks (mTOR IC_{50}: 10 nM for **8a** and **9a**, respectively). For a panel of 5 selected cancer cell lines, **9a** displayed sub-micromolar potencies. In this cell line panel, **9a** was most sensitive to the PIK3CA mutated T47D breast cancer line (IC_{50} = 0.009 μM) and least sensitive to the PTEN null U87 glioblastoma cell line (IC_{50} = 0.30 μM). Relative to **9a**, **8a** showed 3-14 fold lower cellular activity across this cell line panel for the aforementioned permeability reason.

Table 4. *In vitro* profile of **8a** and **9a**.

Assay		**8a**	**9a**
Enzymatic activity IC_{50}[a] (nM)	PI3Kα	1.3	1.1
	PI3Kβ	1.2	3.4
	PI3Kδ	2.7	4.2
	PI3Kγ	10	11
	mTOR	10	10
Cell Growth IC_{50}[b] (μM)	U87MG	2.4	0.30
	T47D	0.13	0.0090
	SKOV3	0.29	0.052
	H460	0.21	0.062
	A549	0.50	0.10
PAMPA	(10^{-6} cm/s)	4.8	9.6
Mouse liver microsome stability	$T_{1/2}$ (min)	139	53
	CL (μL/min/mg)	7.1	19

[a] The IC_{50}s are mean values of duplicates.

[b] The IC_{50}s are mean values of triplicates..

Table 5. Mouse pharmacokinetic parameters of **8a** and **9a**.

Compd	IV (2 mg/kg)[a]			PO (10 mg/kg)[a]			
	$T_{1/2}$ (h)	CL (mL/h/kg)	V_{ss} (mL/kg)	$AUC_{(0-\infty)}$ (h*ng/mL)	Cmax (ng/mL)	$AUC_{(0-\infty)}$ (h*ng/mL)	F (%)
8a	7.7	37	407	54617	10912	186143	67
9a[b]	0.80	351	407	5693	294	1544	6.4
8a[b]	6.9	22	217	91410	1717	34461	/

[a] Three animals per study for IV and five animals per study for PO.

[b] **8a** was a major metabolite of **9a** and blood concentrations of **8a** and **9a** were measured simultaneously to determine their PK parameters after administration of **9a**.

Western blot analysis revealed the effect of **8a** and **9a** on PI3K downstream effectors in NCI-H460 cells (Fig. 2). After 3 hour treatment, **8a** and **9a** inhibited phosphorylation of AKT at S473 and T308, the mTORC1 substrate p70S6K at T389 and the p70S6K substrate S6RP at S235/236 in a dose-dependent manner respectively. **8a** started to show the suppression on phosphorylation from the concentration of 100 nM, while **9a** produced the similar effect from a lower concentration of 30 nM. The data clearly demonstrated **9a** was more potent to inhibit phosphorylation of the PI3K downstream effectors than **8a**, which is consistent with their inhibitory effects on cell proliferation.

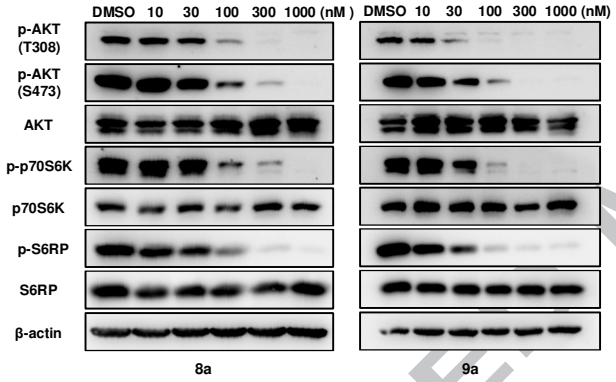

Fig. 2. The PI3K pathway was inhibited by **8a** and **9a** in NCI-H460 cells. The cells were treated with the compounds for 3 hours. Cell lysates were analyzed by Western blot with indicated antibodies. β-actin was used as a loading control.

2.4. Pharmacokinetic study

To measure their in vitro intrinsic clearance, **8a** and **9a** were tested in a mouse microsomal stability assay. **9a** was determined to be moderately stable (CL = 19 μL/min/mg), while **8a** had a much lower clearance rate (CL = 7.1 μL/min/mg). As was also observed in other series,[23] **9a** easily underwent metabolic N-deacetylation to generate the corresponding **8a**, explaining the difference between the microsomal stability in these two compounds.

In vivo pharmacokinetic profile of **8a** and **9a** was examined in mice (Table 5). When **8a** was administrated intravenously at a dose of 2 mg/kg, it exhibited a low clearance (CL = 37 mL/h/kg) and moderate to long half life ($T_{1/2}$ = 7.7 h). After an oral administration at a dose of 10 mg/kg, **8a** demonstrated a very high exposure ($AUC_{(0-\infty)}$ = 186143 h*ng/mL) and good oral bioavailability (F% = 67%). **9a**, however, showed a much higher clearance (CL = 351 mL/h/kg) and shorter half life ($T_{1/2}$ = 0.80 h) in comparison to **8a**. Its $AUC_{(0-\infty)}$ and bioavailability were determined to be 1544 h*ng/mL and 6.4% respectively, significantly lower than those of **8a**. As depicted in supplementary Figure S1, **9a** was metabolically unstable and readily underwent deacetylation in vivo, generating a major active metabolite **8a**. Noteworthy, the overall AUC exposure of metabolite **8a** by oral dosing of **9a** is about 20% of that by orally administrating **8a** itself, while the exposure of metabolite **8a** by intravenous dosing of **9a** is 1.5 fold higher compared to that by dosing of **8a** through the same administration route. These pharmacokinetic studies suggest that **9a** could be considered as a pro-drug of **8a**.

2.5. In vivo efficacy study

Furthermore, **8a** and **9a** were progressed into the established NCI-H460 non-small cell lung cancer (NSCLC) xenograft model. After once-daily oral dosing for 14 consecutive days, **8a** and **9a** exhibited robust and dose-dependent antitumor activity as evidenced by the decrease in tumor volume and tumor weight (Figure 3A and 3B). At the same dose level of 10 mg/kg, **9a** produced a more pronounced in vivo efficacy than **8a** (TGI: 85.2% vs 56.7%). The effect of **8a** and **9a** on phosphorylation of PI3K signaling components was examined by Western blot on day 14. A significant decrease in phosphorylation of AKT at S473 and S6RP at S235/236 was observed in tumor lysates collected 3 hours after last doses (Fig. 3D). **8a** and **9a** were well tolerated over the course of the study. Except for the 10 mg/kg dose of **9a** (14.8% body weight drop), the body weight drop for all the other treatment groups was below 10% compared to their initial weight (Fig. 3C), demonstrating an encouraging safety profile.

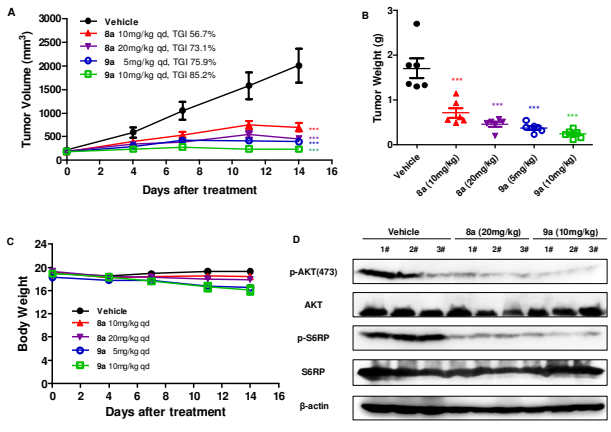

Fig. 3. Antitumor activity of **8a** and **9a** in the NCI-H460 xenograft model. (A) Tumor volume changes. Results are expressed as the mean tumor volume ± SEM (n = 6 for each group). *** p<0.001, vs vehicle. (B) Tumor weight changes at day 14. Results are expressed as tumor weight (n = 6 for each group). *** p<0.001, compared to Vehicle. (C) Body weight changes. Results are expressed as Body Weight ± SEM (n = 6 for each group). (D) Phosphorylation of AKT at S473 and S6RP at S235/236 was significantly

inhibited in the same xenograft model. Tumor lysates were collected 3 hours post doses on the last day.

In a separate *in vivo* study, nude mice bearing NCI-H460 tumors received a single 10mg/kg oral dose of **9a** and pAKT levels in tumor tissues were then determined over the course of 24 hours. As depicted in Fig. 4, **9a** showed a sustained PD response over the 12-hour period with pAKT levels returning to those of control by 24 hour, correlated with the efficacy observed in the NCI-H460 xenograft tumor model.

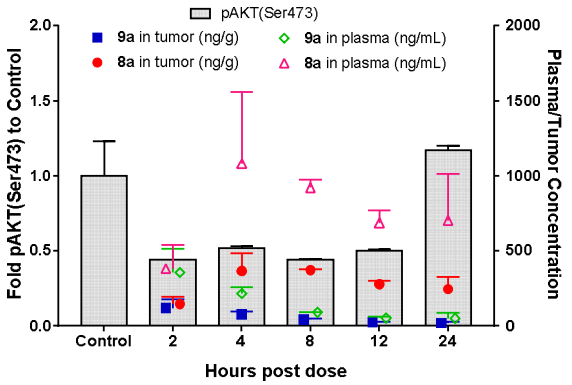

Fig. 4. PD effect of **9a** in the NCI-H460 xenograft model following a single oral dose of 10mg/kg. pAKT (Ser473) levels and compound concentrations (the parent compound **9a** and its metabolite **8a**) in plasma and tumor tissues were measured at 2, 4, 8, 12 and 24 hours post-dose. Error bars denote the standard deviation of the mean (n=3 per group at each time point).

3. Conclusion

In summary, we have described the discovery of a series of new thienopyrimidines as potent PI3K inhibitors. **8a** and **9a** with distinct structures from the series demonstrated nano-molar enzymatic potencies against the Class I PI3K subtypes and sub-micromolar cellular anti-proliferative activities across several cancer cell lines. They could potently suppress phosphorylation of the PI3K downstream effectors including AKT, p70S6K and S6RP. **8a** also displayed favorable pharmacokinetic properties, while **9a** readily underwent deacetylation to afford **8a** as a major active metabolite. Both compounds were efficacious in a dose-dependent manner with an acceptable tolerable safety profile in the NCI-H460 xenograft model. The above findings support further advancement of this new thienopyrimidine series, in particular, **8a** and **9a** into preclinical evaluation.

4. Experimental Section

Unless otherwise noted, all reagents and solvents were from commercial sources. ^{1}H and ^{13}C NMR spectra were recorded on a Varian 300 MHz NMR spectrometer or a Bruker 400 MHz NMR spectrometer. LC-MS spectra were measured with an Agilent LC-MS 6120-1260 instrument. HRMS spectra were measured with Thermo LCQ Deca XP Max mass spectrometer. Melting points were determined on a Yanaco MP-J3 micro melting point apparatus and the maximum temperature was 300 °C. Purity of all compounds tested in biological assays were determined to be >95% by LCMS.

General procedure for the preparation of target compounds

Method A: A mixture of aryl bromide derivatives (1.0 equiv.), 2M aqueous K_2CO_3 solution (4.0 equiv.) and aryl boronic ester (1.2-1.4 equiv.) in dioxane or DMF was degassed, and then $Pd(PPh_3)_2Cl_2$ or $PdCl_2$(dppf) (0.05-0.1 equiv.) was added. The mixture was degassed and back-filled with argon (three cycles), and then stirred at 80-100 °C for 4-6 h. The reaction mixture was diluted with water (50 mL) and extracted with EtOAc (30 mL×3). The combined organic layers were washed with water and brine, dried over Na_2SO_4, filtered and concentrated. The residue was purified by column chromatography (silica gel) to afford the target compounds.

Method B: A mixture of 2,3-disubstituted-5-bromopyridine derivatives (1.2 equiv.), bis(pinacolato)diboron (1.32 equiv.) and potassium acetate (2.4 equiv.) in 1,4-dioxane was degassed, and then $PdCl_2$(dppf) (0.06 equiv.) was added. The reaction mixture was degassed and back-filled with argon (three cycles), stirred at 100 °C under argon atmosphere for 4 h, and then cooled to room temperature. To the resulting mixture was added **13** (1.0 equiv.), 2M aqueous K_2CO_3 solution (3.0 equiv.) and $PdCl_2$(dppf) (0.1 equiv.). The resulting mixture was degassed and back-filled with argon (three cycles) and then stirred at 100 °C under argon atmosphere for 4 h. The reaction mixture was cooled to room temperature, diluted with water (30 mL), and extracted with ethyl acetate (30 mL×3). The combined organic layers were washed with water and brine, dried over anhydrous Na_2SO_4, filtered and concentrated. The residue was purified with column chromatography (silica gel) to afford the target compounds.

***N*-(5-(2-amino-4-methyl-7-oxo-7,8-dihydropyrido[2,3-*d*]pyrimidin-6-yl)-2-methoxypyridin-3-yl)-2,4-difluorobenzenesulfonamide (5)**

Yellow solid (method A, 33% yield). mp: >300 °C. ^{1}H NMR (400 MHz, DMSO-d_6) δ 11.93 (s, 1H), 10.19 (s, 1H), 8.34 (d, J = 2.2 Hz, 1H), 8.02 (s, 1H), 8.00 (d, J = 2.2 Hz, 1H), 7.73 (td, J = 8.4, 2.0 Hz, 1H), 7.62 – 7.56 (m, 1H), 7.20 (td, J = 8.4, 2.0 Hz, 1H), 7.08 (s, 2H), 3.62 (s, 3H), 2.54 (s, 3H). ^{13}C NMR (101 MHz, DMSO-d_6) δ 167.5, 165.0 (dd, J_{C-F} = 255, 11.8 Hz), 162.5, 162.3, 159.4 (dd, J_{C-F} = 259, 13.5 Hz), 157.3, 155.5, 143.9, 136.3, 134.0, 131.8 (d, J_{C-F} = 11.2 Hz), 126.0, 125.1 (dd, J_{C-F} = 14.5, 3.6 Hz), 121.6, 118.5, 111.7 (dd, J_{C-F} = 22.2, 3.0 Hz), 105.7 (t, J_{C-F} = 26.2 Hz), 103.0, 53.2, 20.6, 20.7. HRMS (ESI): m/z [M + H]$^+$ calcd for $C_{20}H_{17}O_4N_6F_2S$, 475.0995, found: 475.0992.

***N*-(5-(2-amino-4,8-dimethyl-7-oxo-7,8-dihydropyrido[2,3-*d*]pyrimidin-6-yl)-2-methoxypyridin-3-yl)-2,4-difluorobenzenesulfonamide (6)**

Yellow solid (method A, 69% yield). mp: 243 – 244 °C. ^{1}H NMR (400 MHz, DMSO-d_6) δ 10.21 (s, 1H), 8.32 (d, J = 2.2 Hz, 1H), 8.05 (s, 1H), 8.01 (d, J = 2.2 Hz, 1H), 7.72 (td, J = 8.6, 6.4 Hz, 1H), 7.63 – 7.53 (m, 1H), 7.26 (s, 2H), 7.20 (td, J = 8.4, 2.2 Hz, 1H), 3.62 (s, 3H), 3.58 (s, 3H), 2.57 (s, 3H). ^{13}C NMR (101 MHz, DMSO-d_6) δ 168.0, 165.0 (dd, J_{C-F} = 255, 11.8 Hz), 162.0, 161.7, 159.4 (dd, J_{C-F} = 259, 13.5 Hz), 157.3, 155.3, 144.1, 136.6, 132.7, 131.9 (d, J_{C-F} = 10.7 Hz), 126.4, 125.2 (dd, J_{C-F} = 14.5, 3.5 Hz), 120.5, 118.3, 111.7 (dd, J_{C-F} = 22.3, 3.2 Hz), 105.8 (t, J_{C-F} = 26.3 Hz), 103.3, 53.2, 28.0, 20.7. HRMS (ESI): m/z [M + H]$^+$ calcd for $C_{21}H_{19}O_4N_6F_2S$, 489.1151, found: 489.1146.

***N*-(5-(2-amino-4,8-dimethyl-7-oxo-7,8-dihydropteridin-6-yl)-2-methoxypyridin-3-yl)-2,4-difluorobenzenesulfonamide (7)**

Yellow solid (method A, 66% yield). mp: 269 – 271 °C. ^{1}H NMR (400 MHz, DMSO-d_6) δ 10.32 (s, 1H), 8.99 (d, J = 2.1 Hz, 1H), 8.40 (d, J = 2.1 Hz, 1H), 7.76 (td, J = 8.6, 6.4 Hz, 1H), 7.64 – 7.54 (m, 1H), 7.43 (s, 2H), 7.23 (td, J = 8.4, 2.4 Hz, 1H), 3.71 (s, 3H), 3.54 (s, 3H), 2.60 (s, 3H). ^{13}C NMR (101 MHz, DMSO-

d_6) δ 168.6, 165.1 (dd, $J_{C\text{-}F}$ = 255, 11.8 Hz), 161.6, 159.4 (dd, $J_{C\text{-}F}$ = 259, 13.5 Hz), 158.2, 156.0, 149.5, 144.9, 141.6, 134.8, 131.9 (d, $J_{C\text{-}F}$ = 10.7 Hz), 126.0, 125.1 (dd, $J_{C\text{-}F}$ = 14.3, 3.7 Hz), 119.0, 117.8, 111.9 (dd, $J_{C\text{-}F}$ = 22.3, 2.9 Hz), 105.9 (t, $J_{C\text{-}F}$ = 26.2 Hz), 53.6, 27.1, 18.9. HRMS (ESI): m/z $[M + H]^+$ calcd for $C_{20}H_{18}O_4N_7F_2S$, 490.1104, found: 490.1096.

_N_-(5-(2-amino-4-methylthieno[2,3-_d_]pyrimidin-6-yl)-2-methoxypyridin-3-yl)-2,4-difluorobenzenesulfonamide (8a).

White solid (method A, 48% yield). mp: 229 – 230 °C. ^{1}H NMR (400 MHz, DMSO-d_6) δ 10.33 (s, 1H), 8.32 (d, J = 2.4 Hz, 1H), 7.91 (d, J = 2.4 Hz, 1H), 7.82 – 7.71 (m, 2H), 7.58 (ddd, J = 10.4, 9.2, 2.4 Hz, 1H), 7.22 (td, J = 8.4, 2.0 Hz, 1H), 6.81 (s, 2H), 3.63 (s, 3H), 2.57 (s, 3H). ^{13}C NMR (101 MHz, DMSO-d_6) δ 169.6, 165.1 (dd, $J_{C\text{-}F}$ = 255, 11.8 Hz), 162.9, 160.6, 159.4 (dd, $J_{C\text{-}F}$ = 259, 13.6 Hz), 157.6, 141.1, 132.8, 131.9 (d, $J_{C\text{-}F}$ = 10.9 Hz), 129.5, 125.0 (dd, $J_{C\text{-}F}$ = 14.5, 3.6 Hz), 124.0, 122.4, 119.8, 117.0, 111.9 (dd, $J_{C\text{-}F}$ = 22.2, 3.3 Hz), 105.8 (t, $J_{C\text{-}F}$ = 26.2 Hz), 53.5, 21.7. HRMS (ESI): m/z $[M + H]^+$ calcd for $C_{19}H_{16}O_3N_5F_2S_2$, 464.0657, found: 464.0649.

_N_-(5-(2-amino-4-methylthieno[2,3-_d_]pyrimidin-6-yl)-2-methoxypyridin-3-yl)-4-fluorobenzenesulfonamide (8b)

White solid (method A, 38% yield). mp: 259 – 261 °C. ^{1}H NMR (400 MHz, DMSO-d_6) δ 10.07 (s, 1H), 8.30 (d, J = 2.4 Hz, 1H), 7.85 (d, J = 2.4 Hz, 1H), 7.82 (dd, J = 8.8, 5.2 Hz, 2H), 7.72 (s, 1H), 7.42 (t, J = 8.8 Hz, 2H), 6.81 (s, 2H), 3.64 (s, 3H), 2.57 (s, 3H). ^{13}C NMR (101 MHz, DMSO-d_6) δ 169.5, 164.4 (d, $J_{C\text{-}F}$ = 253 Hz), 162.8, 160.5, 156.6, 140.3, 136.5 (d, $J_{C\text{-}F}$ = 2.8 Hz), 130.6, 129.8 (d, $J_{C\text{-}F}$ = 9.7 Hz), 123.8, 122.4, 120.5, 116.8, 116.2 (d, $J_{C\text{-}F}$ = 22.9 Hz), 53.6, 21.8. HRMS (ESI): m/z $[M + H]^+$ calcd for $C_{19}H_{17}O_3N_5FS_2$, 446.0751, found: 446.0745.

_N_-(5-(2-amino-4-methylthieno[2,3-_d_]pyrimidin-6-yl)-2-methoxypyridin-3-yl)-5-chlorothiophene-2-sulfonamide (8c)

Yellow solid (method A, 43% yield). mp: 239 – 240 °C. ^{1}H NMR (400 MHz, DMSO-d_6) δ 10.37 (s, 1H), 8.37 (d, J = 2.4 Hz, 1H), 7.89 (d, J = 2.4 Hz, 1H), 7.76 (s, 1H), 7.40 (d, J = 4.0 Hz, 1H), 7.24 (d, J = 4.0 Hz, 1H), 6.81 (s, 2H), 3.73 (s, 3H), 2.57 (s, 3H). ^{13}C NMR (101 MHz, DMSO-d_6) δ 169.6, 162.9, 160.6, 157.2, 140.9, 138.9, 135.4, 132.4, 131.6, 129.5, 127.9, 124.0, 122.4, 120.0, 116.9, 53.7, 21.8. HRMS (ESI): m/z $[M + H]^+$ calcd for $C_{17}H_{15}O_3N_5ClS_3$, 468.0020, found: 468.0019.

_N_-(5-(2-amino-4-methylthieno[2,3-_d_]pyrimidin-6-yl)-2-methoxypyridin-3-yl)methanesulfonamide (8d)

White solid (method A, 53% yield). mp: 278 – 280 °C. ^{1}H NMR (400 MHz, DMSO-d_6) δ 9.40 (s, 1H), 8.32 (d, J = 2.3 Hz, 1H), 7.92 (d, J = 2.3 Hz, 1H), 7.75 (s, 1H), 6.81 (s, 2H), 3.96 (s, 3H), 3.10 (s, 3H), 2.57 (s, 3H). ^{13}C NMR (101 MHz, DMSO-d_6) δ 169.5, 162.8, 160.5, 156.4, 139.5, 129.9, 129.4, 124.0, 122.4, 121.6, 116.7, 53.9, 40.8, 21.8. HRMS (ESI): m/z $[M + H]^+$ calcd for $C_{14}H_{16}O_3N_5S_2$, 366.0689, found: 366.0686.

_N_-(5-(2-amino-4-methylthieno[2,3-_d_]pyrimidin-6-yl)-2-methoxypyridin-3-yl)cyclopropanesulfonamide (8e)

White solid (method A, 59% yield). mp: 254 – 255 °C. ^{1}H NMR (400 MHz, DMSO-d_6) δ 9.43 (s, 1H), 8.32 (d, J = 2.3 Hz, 1H), 7.93 (d, J = 2.3 Hz, 1H), 7.74 (s, 1H), 6.81 (s, 2H), 3.96 (s, 3H), 2.80 – 2.72 (m, 4H), 2.57 (s, 3H), 1.00 – 0.87 (m, 4H). ^{13}C NMR (101 MHz, DMSO-d_6) δ 169.6, 162.8, 160.5, 156.7, 139.6, 129.9, 129.7, 123.9, 122.4, 121.7, 116.7, 53.9, 30.5, 21.8, 5.1. HRMS (ESI): m/z $[M + H]^+$ calcd for $C_{16}H_{18}O_3N_5S_2$, 392.0846; found: 392.0840.

_N_-(5-(2-amino-4-methylthieno[2,3-_d_]pyrimidin-6-yl)-2-chloropyridin-3-yl)-4-fluorobenzenesulfonamide (8f)

White solid (method B, 46% yield). mp: 280 – 281 °C. ^{1}H NMR (400 MHz, DMSO-d_6) δ 10.52 (s, 1H), 8.53 (s, 1H), 7.92 (s, 1H), 7.84 – 7.78 (m, 3H), 7.42 (t, J = 8.8 Hz, 2H), 6.92 (s, 2H), 2.58 (s, 3H). ^{13}C NMR (100 MHz, DMSO-d_6) δ 170.0, 164.6 (d, $J_{C\text{-}F}$ = 253 Hz), 163.7, 160.8, 144.5, 143.3, 136.3 (d, $J_{C\text{-}F}$ = 2.8 Hz), 132.2, 130.7, 129.91, 129.90 (d, $J_{C\text{-}F}$ = 9.8 Hz), 127.7, 122.2, 119.6, 116.7 (d, $^2J_{C\text{-}F}$ = 23 Hz), 21.8. HRMS (ESI): m/z $[M + H]^+$ calcd for $C_{18}H_{14}O_2N_5ClFS_2$, 450.0256, found: 450.0248.

_N_-(5-(2-amino-4-methylthieno[2,3-_d_]pyrimidin-6-yl)-2-methylpyridin-3-yl)-4-fluorobenzenesulfonamide (8g)

White solid (method B, 40% yield). mp: >300 °C. ^{1}H NMR (300 MHz, DMSO-d_6) δ 10.05 (s, 1H), 8.70 (d, J = 2.0 Hz, 1H), 7.82 (s, 1H), 7.76 (dd, J = 8.8, 5.2 Hz, 2H), 7.49 (d, J = 2.0 Hz, 1H), 7.46 (t, J = 8.8 Hz, 2H), 6.87 (s, 2H), 2.57 (s, 3H), 2.17 (s, 3H). HRMS (ESI): m/z $[M + H]^+$ calcd for $C_{19}H_{17}O_2N_5FS_2$, 430.0802, found: 430.0795.

_N_-(5-(2-amino-4-methylthieno[2,3-_d_]pyrimidin-6-yl)-2-methylpyridin-3-yl)-2,4-difluorobenzenesulfonamide (8h)

Pale yellow solid (method B, 28% yield). mp: 275 – 277 °C. ^{1}H NMR (400 MHz, DMSO-d_6) δ 10.49 (br s, 1H), 8.68 (s, 1H), 7.85 – 7.74 (m, 2H), 7.65 – 7.56 (m, 2H), 7.26 (td, J = 8.6, 2.1 Hz, 1H), 6.87 (s, 2H), 2.57 (s, 3H), 2.29 (s, 3H). HRMS (ESI): m/z $[M + H]^+$ calcd for $C_{19}H_{16}O_2N_5F_2S_2$, 448.0708, found: 448.0702.

_N_-(6-(5-(2,4-difluorophenylsulfonamido)-6-methoxypyridin-3-yl)-4-methylthieno[2,3-_d_]pyrimidin-2-yl)acetamide (9a).

White solid (method A, 42% yield). mp: 254 – 256 °C. ^{1}H NMR (400 MHz, DMSO-d_6) δ 10.67 (s, 1H), 10.39 (s, 1H), 8.44 (d, J = 2.4 Hz, 1H), 8.03 (d, J = 2.4 Hz, 1H), 8.02 (s, 1H), 7.78 (td, J = 8.6, 6.4 Hz, 1H), 7.59 (ddd, J = 10.6, 9.2, 2.4 Hz, 1H), 7.23 (td, J = 8.4, 2.4 Hz, 1H), 3.65 (s, 3H), 2.74 (s, 3H), 2.20 (s, 3H). ^{13}C NMR (101 MHz, DMSO-d_6) δ 168.8, 167.9, 165.1 (dd, $J_{C\text{-}F}$ = 255, 11.8 Hz), 163.0, 159.4 (dd, $J_{C\text{-}F}$ = 258, 13.3 Hz), 158.1, 153.5, 141.8, 135.3, 133.1, 131.9 (d, $J_{C\text{-}F}$ = 10.9 Hz), 126.9, 125.0 (dd, $J_{C\text{-}F}$ = 14.5, 3.5 Hz), 123.3, 120.0, 116.7, 111.9 (dd, $J_{C\text{-}F}$ = 22.6, 2.7 Hz), 105.8 (d, $J_{C\text{-}F}$ = 26.2 Hz), 53.6, 24.6, 21.8. HRMS (ESI): m/z $[M + H]^+$ calcd for $C_{21}H_{18}O_4N_5F_2S_2$, 506.0763, found: 506.0754.

_N_-(6-(5-((2,4-difluorophenyl)sulfonamido)-6-methoxypyridin-3-yl)-4-methylthieno[2,3-_d_]pyrimidin-2-yl)propionamide (9b)

Pale yellow solid (method A, 40% yield). mp: 173 – 175 °C. ^{1}H NMR (400 MHz, DMSO-d_6) δ 10.63 (s, 1H), 10.39 (s, 1H), 8.44 (d, J = 2.4 Hz, 1H), 8.03 (d, J = 2.4 Hz, 1H), 8.01 (s, 1H), 7.78 (dd, J = 8.4, 2.4 Hz, 1H), 7.64 – 7.54 (m, 1H), 7.23 (td, J = 8.0, 1.6 Hz, 1H), 3.65 (s, 3H), 2.74 (s, 3H), 2.50 (q, J = 7.4 Hz, 2H), 1.07 (t, J = 7.4 Hz, 3H). ^{13}C NMR (101 MHz, DMSO-d_6) δ 172.2, 167.9, 165.1 (dd, $J_{C\text{-}F}$ = 255, 11.8 Hz), 162.9, 159.4 (dd, $J_{C\text{-}F}$ = 258, 13.5 Hz), 158.1, 153.5, 141.7, 135.2, 133.1, 131.9 (d, $J_{C\text{-}F}$ = 11.0 Hz), 126.9, 125.0 (dd, $J_{C\text{-}F}$ = 14.4, 3.6 Hz), 123.3, 120.0, 116.6, 111.9 (dd, $J_{C\text{-}F}$ = 22.4, 3.3 Hz), 105.8 (d, $J_{C\text{-}F}$ = 26.2 Hz), 53.6, 29.7, 21.8, 9.2. HRMS (ESI): m/z $[M + H]^+$ calcd for $C_{22}H_{20}O_4N_5F_2S_2$, 520.0919, found: 520.0915.

_N_-(6-(5-((2,4-difluorophenyl)sulfonamido)-6-methoxypyridin-3-yl)-4-methylthieno[2,3-_d_]pyrimidin-2-yl)butyramide (9c)

Pale yellow solid (method A, 49% yield). mp: 178 – 179 °C. ^{1}H NMR (400 MHz, DMSO-d_6) δ 10.64 (s, 1H), 10.39 (s, 1H), 8.44 (d, J = 2.0 Hz, 1H), 8.03 (d, J = 2.0 Hz, 1H), 8.02 (s, 1H), 7.78 (dd, J = 8.0, 2.8 Hz, 1H), 7.63 – 7.54 (m, 1H), 7.23 (td, J =

8.4, 1.2 Hz, 1H), 3.65 (s, 3H), 2.74 (s, 3H), 2.46 (t, J = 7.2 Hz, 2H), 1.68 – 1.53 (m, 2H), 0.92 (t, J = 7.4 Hz, 3H). ^{13}C NMR (101 MHz, DMSO-d_6) δ 171.2, 167.9, 165.1 (dd, $J_{C\text{-}F}$ = 255, 11.8 Hz), 163.0, 159.4 (dd, $J_{C\text{-}F}$ = 259, 13.7 Hz), 158.1, 153.4, 141.7, 135.3, 133.2, 131.9 (d, $J_{C\text{-}F}$ = 10.8 Hz), 126.9, 125.0 (dd, $J_{C\text{-}F}$ = 14.3, 3.6 Hz), 123.3, 120.0, 116.7, 111.9 (dd, $J_{C\text{-}F}$ = 22.2, 3.2 Hz), 105.8 (d, $J_{C\text{-}F}$ = 26.2 Hz), 53.6, 38.3, 21.8, 18.2, 13.6. HRMS (ESI): m/z [M + H]$^+$ calcd for $C_{23}H_{22}O_4N_5F_2S_2$, 534.1076, found: 534.1072.

***N*-(6-(5-((2,4-difluorophenyl)sulfonamido)-6-methoxypyridin-3-yl)-4-methylthieno[2,3-*d*]pyrimidin-2-yl)cyclopropanecarboxamide (9d)**

White solid (method A, 37% yield). mp: 138 – 139 °C. ^{1}H NMR (400 MHz, DMSO-d_6) δ 11.03 (s, 1H), 10.42 (s, 1H), 8.45 (d, J = 2.4 Hz, 1H), 8.04 (s, 1H), 8.03 (d, J = 2.4 Hz, 1H), 7.77 (td, J = 8.4, 6.4 Hz, 1H), 7.64 – 7.56 (m, 1H), 7.23 (td, J = 8.4, 2.0 Hz, 1H), 3.65 (s, 3H), 2.75 (s, 3H), 2.17 – 2.07 (m, 1H), 0.88 – 0.76 (m, 4H). ^{13}C NMR (101 MHz, DMSO-d_6) δ 171.6, 167.9, 165.1 (dd, $J_{C\text{-}F}$ = 255, 11.8 Hz), 163.0, 159.4 (dd, $J_{C\text{-}F}$ = 256, 13.3 Hz), 158.1, 153.3, 141.8, 135.3, 133.2, 131.9 (d, $J_{C\text{-}F}$ = 10.8 Hz), 127.0, 125.0 (dd, $J_{C\text{-}F}$ = 14.4, 3.6 Hz), 123.3, 120.0, 116.7, 111.9 (dd, $J_{C\text{-}F}$ = 22.4, 3.3 Hz), 105.8 (d, $J_{C\text{-}F}$ = 26.3 Hz), 53.6, 21.8, 14.4, 8.0. HRMS (ESI): m/z [M + H]$^+$ calcd for $C_{23}H_{20}O_4N_5F_2S_2$, 532.0919, found: 532.0917.

***N*-(2-methoxy-5-(4-methyl-2-(methylamino)thieno[2,3-*d*]pyrimidin-6-yl)pyridin-3-yl)2,4-difluorobenzenesulfonamide (9e)**

Yellow solid (method A, 40% yield). mp: 272 – 273 °C. ^{1}H NMR (400 MHz, DMSO-d_6) δ 10.34 (s, 1H), 8.32 (d, J = 2.2 Hz, 1H), 7.91 (d, J = 2.2 Hz, 1H), 7.82 – 7.72 (m, 2H), 7.64 – 7.53 (m, 1H), 7.30 (br s, 1H), 7.22 (td, J = 8.7, 2.5 Hz, 1H), 3.63 (s, 3H), 2.85 (d, J = 4.8 Hz, 3H), 2.58 (s, 3H). ^{13}C NMR (101 MHz, DMSO-d_6) δ 169.5, 165.1 (dd, $J_{C\text{-}F}$ = 255, 11.8 Hz), 162.6, 160.0, 159.4 (dd, $J_{C\text{-}F}$ = 259, 13.4 Hz), 157.5, 141.0, 132.8, 131.9 (d, $J_{C\text{-}F}$ = 10.7 Hz), 129.3, 125.0 (dd, $J_{C\text{-}F}$ = 14.4, 3.6 Hz), 124.0, 122.2, 119.8, 117.0, 111.9 (dd, $J_{C\text{-}F}$ = 22.3, 3.2 Hz), 105.8 (t, $J_{C\text{-}F}$ = 26.3 Hz), 53.5, 28.0, 21.9. HRMS (ESI): m/z [M + H]$^+$ calcd for $C_{20}H_{18}O_3N_5F_2S_2$, 478.0814, found: 478.0808.

***N*-(6-(5-(5-chlorothiophene-2-sulfonamido)-6-methoxypyridin-3-yl)-4-methylthieno[2,3-*d*]pyrimidin-2-yl)acetamide (9f)**

Pale yellow solid (method A, 40% yield). mp: 223 – 224 °C. ^{1}H NMR (400 MHz, DMSO-d_6) δ 10.69 (s, 1H), 10.45 (s, 1H), 8.48 (d, J = 2.4 Hz, 1H), 8.02 (s, 1H), 8.01 (d, J = 2.4 Hz, 1H), 7.42 (d, J = 4.1 Hz, 1H), 7.25 (d, J = 4.1 Hz, 1H), 3.75 (s, 3H), 2.74 (s, 3H), 2.20 (s, 3H). ^{13}C NMR (101 MHz, DMSO-d_6) δ 168.8, 167.9, 163.0, 157.6, 153.4, 141.6, 138.8, 135.4, 132.4, 131.9, 127.9, 126.9, 123.3, 120.1, 116.6, 53.8, 24.6, 21.9. HRMS (ESI): m/z [M + H]$^+$ calcd for $C_{19}H_{17}O_4N_5ClS_2$, 510.0126, found: 510.0123.

***N*-(6-(6-methoxy-5-(methylsulfonamido)pyridin-3-yl)-4-methylthieno[2,3-*d*]pyrimidin-2-yl)acetamide (9g)**

Pale yellow solid (method A, 20% yield). mp: 225 – 227 °C. ^{1}H NMR (400 MHz, DMSO-d_6) δ 10.67 (s, 1H), 9.46 (s, 1H), 8.43 (d, J = 2.3 Hz, 1H), 8.01 (d, J = 2.3 Hz, 1H), 7.99 (s, 1H), 3.98 (s, 3H), 3.11 (s, 3H), 2.74 (s, 3H), 2.20 (s, 3H). ^{13}C NMR (101 MHz, DMSO-d_6) δ 168.8, 167.9, 162.9, 157.0, 153.4, 140.2, 135.8, 129.7, 127.0, 123.3, 121.8, 116.5, 54.0, 40.9, 24.6, 21.9. HRMS (ESI): m/z [M + H]$^+$ calcd for $C_{16}H_{18}O_4N_5S_2$, 408.0795, found: 408.0789.

PI3Kα Biochemical Assay

Kinase-Glo™ kinase detection kit was from Promega. PI3Kα kinase was and the substrate PIP2 was from Invitrogen. All assays were performed on a 384-well plate at room temperature. The kinase buffer contained 50 mM Hepes (pH 7.5), 3 mM $MgCl_2$, 100 mM NaCl, 1 mM EGTA, 0.03% CHAPS and 2 mM DTT. PI3Kα kinase solution was prepared by diluting PI3Kα in the kinase buffer to 6.6 nM. The ATP/substrate solution contained 100 μM PIP2 and 50 μM ATP. Compounds for testing were diluted into 10 mM in 100% DMSO then serially diluted 3-fold in 100% DMSO at 10 different concentrations. Then the diluted compounds in 100% DMSO were 25-fold diluted in the kinase buffer. 2.5 μL of diluted compound solution and 2.5 μL of PI3Kα kinase solution were added to individual wells of 384-well assay plates. The reactions were started by adding 5 μL of ATP/substrate solution per well. The final volume for the reaction was 10 μL, ATP concentration was 25 μM, PIP2 concentration was 50 μM, and PI3Kα kinase concentration was 1.65 nM. The assay plates were covered and reactions were allowed to proceed for 1 hour, after which 10 μL of Kinase-Glo™ reagent per well was added. The plates were incubated for 15 minutes, after which luminescence was measured using an Envision plate reader. IC_{50} values were determined by curve fitting using XLfit program of Excel software (Microsoft, USA).

Proliferation assays

Compounds were evaluated for antiproliferative potency against U87MG, T47D, SKOV3, H460 and A549 tumor cell lines using a CellTiter-Glo® Luminescent Cell Viability Assay from Promega. The human tumor cell lines used were obtained from the ATCC. All the mediums and FBS were Gibco. T47D and H460 tumor cells were cultured in RPMI1640 medium supplemented with 10% FBS. SKOV3 ovarian cancer cells were cultured in McCoy's 5a medium supplemented with 10% FBS. U87MG were cultured in DMEM medium supplemented with 10% FBS. A549 were cultured in Ham's F12K medium supplemented with 10% FBS.Tumor cells were seeded at a volume of 80 μL/well and a density of 3000 cells/well in 96-well plates and subsequently incubated at 37 °C and 5% CO_2 for 2 hours. Compounds for testing were diluted into 10 mM in 100% DMSO then serially diluted 3.16-fold in 100% DMSO at 10 different concentrations. Then the diluted compounds in 100% DMSO were 20-fold diluted in 100% DMSO. The tumor cells were then treated with serially diluted compound or DMSO control in the incubator at 37 °C and 5% CO_2 for 4 days, prior to the addition of CellTiter-Glo reagents (Promega) and reading of luminescence using a PerkinElmer Envision plate reader. IC_{50} values were determined by curve fitting using XLfit program of Excel software (Microsoft, USA).

Parallel artificial membrane permeation assay (PAMPA)

The pre-coated PAMPA plate system (BD Gentest) was used to evaluate the effective permeabilities (P_e) of compounds. The working solutions of compounds were added in the receiver plate (donor plate) while the blank buffer added in the filter plate (acceptor plate). The filter plate was assembled on the receiver plate by slowly lowering the pre-coated PAMPA plate, which was then incubated at room temperature for 5 hours. After the incubation, aliquots from donor and acceptor plates were delivered to LC/MS/MS analysis. The Waters UPLC system coupling to an API 4000 MS instrument was used for the LC/MS/MS analysis with a Waters UPLC AQURITY BEH C18 column.

Immunoblotting

NCI-H460 cancer cells (ATCC) were exposed to compounds for 3 hours. Cells were collected and then lysed in a buffer

containing 1% sodium dodecyl sulfate (SDS), 10 mM ethylenediaminetetraacetic acid (EDTA), 50 mM Tris–HCl (pH 8.1), 1% proteinase inhibitor cock tails and 1% protease inhibitor mixture. Lysates were sonicated and then centrifuged at 13,000g for 10 min. Protein concentrations in the supernatants were determined (Micro BCA Protein Assay Kit, Pierce Biotechnology, Rockford, IL). Equal amounts of proteins were resolved in an SDS–polyacrylamide gel and transferred to a polyvinylidene fluoride membrane (Merck Millipore). The membrane was washed twice with Tris-buffered saline containing 0.1% Tween-20 (TBST), blocked with TBST containing 5% non-fat milk for 30 min, and then incubated with primary antibody (1:500–1:4000 dilution) in TBST at 4 °C overnight. AKT, phosphor-Akt (S473), phosphor-Akt (T308), p70S6K, phosphor-p70S6K, S6RP, phosphor-S6RP antibodies were obtained from CST and actin antibody was from Santa Cruz. After washing with TBST, the membrane was incubated with goat anti-rabbit or anti-mouse IgG–HRP conjugates (1:5000 dilution, Origene ZB-2301 or ZB-2305) for 1 h at room temperature. The immunoblots were visualized by enhanced chemiluminescence.

Mouse liver microsome stability Assay

Mouse liver microsomes were purchased from Xenotech. Compounds with a final concentration of 1.11 μM were incubated with NADP co-factor solution and mouse liver microsome (final concentration 0.7 mg protein/mL) at 37 °C for 0min, 10min, 30min, 60min and 90min respectively. Samples were then quenched with acetonitrile and centrifuged for 20min at 4000rpm. The supernatants were analyzed by LC/MS/MS.

Pharmacokinetic study

Test compounds were subjected to pharmacokinetic studies on male ICR mice. For oral administration, five animals were in each group and three animals were in each group for intravenous administration. The test compounds were orally administered as 0.1%PEG400/0.5%CMC suspension (10 mg/kg) or intravenous injected as 10%DMSO saline (2 mg/kg). Blood samples were collected at 0.083, 0.25, 0.5, 1, 2, 4, 6, 8, 12 and 24 h time points following oral dosing and at 0.033, 0.083, 0.25, 0.5, 1, 2, 4, 6, 8, 12 and 24 h following intravenous dosing. The concentrations of test compounds were determined by high pressure liquid chromatography/tandem mass spectrometry (LC/MS/MS). Relevant pharmacokinetic parameters were derived by non-compartmental pharmacokinetic analysis (WinNonlin).

***In vivo* antitumor activity study**

Female athymic BALB/c nude mice (8–10 week old) were purchased from Vital River Laboratories, Beijing, China. A total of 1×10^6 NCI-H460 cells in 0.1 mL sterilized PBS were implanted subcutaneously in mice. When the tumor volume reached to 1000 mm^3, the tumor issues were cut into 1.5 mm^3 fragments and transplanted subcutaneously into the right flank of nude mice using a tracer. After 7 days, the mice were grouped (6 mice/group) with tumor volumes at 100-300 mm^3 and received treatment. The test compounds (in 0.5% CMC) were administrated orally once daily for 14 days. Body weights and tumor volumes (TV) were measured twice every week. The mice were euthanized 3 hours later after final dose at Day 14. Tumor issues were collected and weighted. The proteins of tumor tissues were tested following immunoblotting procedure as above. TV was calculated as (length × $width^2$)/2. The relative tumor volume (RTV) was calculated as V_t/V_0 for both treatment groups and vehicle group, while V_0 is the tumor volume at day 0, V_t is the tumor volume measured each time point. Tumor volume inhibition (TGI) at Day 14 was measured as (1-$RTV_{treatment}/RTV_{vehicle}$) ×100%. Statistical analyses were performed by GraphPad Prism5 software and the significance levels were evaluated using one-way ANOVA model.

PK-PD study

Female athymic BALB/c nude mice (8–10 week old) were implanted with NCI-H460 tumor cells. When the tumor volumes reached to 500-600 mm^3, mice were administered orally (via gavage) at a single dose of 10mg/kg. At different time points as indicated, animals were anaesthetized and sacrificed. Blood and tumor samples were collected. Blood samples were centrifuged to obtain the plasma for PK analysis. Tumor tissues were homogenized for PK analysis. For Akt (Ser 473) phosphorylation analysis, it follows the protocol of phospho-AKT (S473) ELISA Kit (Abcam, ab176657). The data was analyzed by Graphpad Prism 7.

Acknowledgments

This work was supported in part by CAMS Innovation Fund for Medical Sciences (grant no. 2017-I2M-3-011).

Supplementary Material

The procedures for the preparation of synthetic intermediates and biological evaluations are reported in the supplementary data.

References

1. Vivanco, I.; Sawyers, C. L. The phosphatidylinositol 3-Kinase-AKT pathway in human cancer. *Nat. Rev. Cancer* **2002**, *2*, 489–501.
2. Engelman, J. A.; Luo, J.; Cantley, L. C. The evolution of phosphatidylinositol 3-kinases as regulators of growth and metabolism. *Nat. Rev. Genet.* **2006**, *7*, 606–619.
3. Liu, P. X; Cheng, H. L.; Roberts, T. M.; Zhao, J. J. Targeting the phosphoinositide 3-kinase pathway in cancer. *Nat. Rev. Drug Discov.* **2009**, *8*, 627–644.
4. Sarbassov, D. D.; Ali, S. M.; Sabatini, D. M. Growing roles for the mTOR pathway. *Curr. Opin. Cell Biol.* **2005**, *17*, 596-603.
5. Song, M. S.; Salmena, L.; Pandolfi, P. P. The functions and regulation of the PTEN tumour suppressor. *Nat. Rev. Mol. Cell Biol.* **2012**, *13*, 283–296.
6. Engelman, J. A. Targeting PI3K signalling in cancer: opportunities, challenges and limitations. *Nat. Rev. Cancer* **2009**, *9*, 550–562.
7. Yuan, T. L; Cantley, L. C. PI3K pathway alterations in cancer: variations on a theme. *Oncogene* **2008**, *27*, 5497–5510.
8. Millis, S. Z.; Ikeda, S.; Reddy, S.; Gatalica, Z.; Kurzrock, R. Landscape of phosphatidylinositol-3-kinase pathway alterations across 19 784 diverse solid tumors. *JAMA Oncol.* **2016**, *2*, 1565–1573.
9. Shuttleworth, S. J.; Silva, F. A.; Cecil, A. R. L.; Tomassi, C. D.; Hill, T. J.; Raynaud, F. I.; Clarke, P. A.; Workman, P. Progress in the preclinical discovery and clinical development of class I and dual class I/IV phosphoinositide 3-kinase (PI3K) inhibitors. *Curr. Med. Chem.* **2011**, *18*, 2686–2714 and the references therein.
10. Brana, I.; Siu, L. L. Clinical development of phosphatidylinositol 3-kinase inhibitors for cancer treatment. *BMC Med.* **2012**, *10*, 161 and the references therein.
11. Lomon So, L.; Fruman D. A. PI3K signaling in B and T lymphocytes: new developments and therapeutic advances. *Biochem. J.* **2012**, *442*, 465–481 and the references therein.
12. Yap, T. A.; Bjerke, L.; Clarke, P. A.; Workman, P. Drugging PI3K in cancer: refining targets and therapeutic strategies. *Curr. Opin. Pharmaco.* **2015**, *23*, 98–107 and the references therein.
13. http://www.fda.gov/drugs/informationondrugs/approveddrugs/ucm406410.htm
14. https://www.fda.gov/NewsEvents/Newsroom/PressAnnouncements/ucm576129.htm

15. Scott, W. J.; Hentemann, M. F.; Rowley, R. B.; Bull, C. O.; Jenkins, S.; Bullion, A. M.; Johnson, J.; Redman, A.; Robbins, A. H.; Esler, W.; Fracasso, R. P.; Garrison, T.; Hamilton, M.; Michels, M.; Wood, J. E.; Wilkie, D. P.; Xiao, H.; Levy, J.; Stasik, E.; Liu, N.; Schaefer, M.; Brands, M.; Lefranc,J. Discovery and SAR of novel 2,3-dihydroimidazo[1,2-*c*]quinazoline PI3K inhibitors: identification of Copanlisib (BAY 80-6946). *Chem. Med. Chem.* **2016**, *11*, 1517–1530.
16. Fruman, D. A.; Rommel, C. PI3K and cancer: lessons, challenges and opportunities. *Nat. Rev. drug discov.* **2014**, *13*, 140-156.
17. Rodon, J.; Dienstmann, R.; Serra, V.; Tabernero, J. Development of PI3K inhibitors: lessons learned from early clinical trials. *Nat. Rev. Clin. Oncol.* **2013**, *10*, 143–153.
18. Thorpe, L. M.; Yuzugullu ,H.; Zhao, J. J. PI3K in cancer: divergent roles of isoforms, modes of activation and therapeutic targeting. *Nat. Rev. Cancer* **2015**, *15*, 7–24.
19. Han, F.; Lin, S.; Liu, P.; Tao, J.; Yi, C. Q.; Xu, H. Synthesis and structure-activity relationships of PI3K/mTOR dual inhibitors from a series of 2-amino-4-methylpyrido[2,3-*d*]pyrimidine derivatives. *Bioorg. Med. Chem. Lett*. **2014**, *24*, 4538–4541.
20. Kun, P.-P.; Meng, J. J. 2-Amino pyridine compounds. Int. PCT Pub. No. WO2008/059368 A2, **2008**.
21. Knight, S. D.; Adams, N. D.; Burgess, J. L.; Chaudhari, A. M.; Darcy, M. G.; Donatelli, C. A.; Luengo, J. I.; Newlander, K. A.; Parrish, C. A.; Ridgers, L.; Sarpong, M. A.; Schmidt, S. J.; Van Aller, G. S.; Carson, J. D.; Diamond, M. A.; Elkins, P. A.; Gardiner, C. M.; Garver, E.; Gilbert, S. A.; Gontarek, R. R.; Jackson, J. R.; Kershner, K. L.; Luo, L.; Raha, K.; Sherk, C. S.; Sung, C.; Sutton, D.; Tummino, P. J.; Wegrzyn, R. J.; Auger, K. R.; Dhanak, D. Discovery of GSK2126458, a highly potent inhibitor of PI3K and the mammalian target of rapamycin. *ACS Med. Chem. Lett.* **2010**, *1*, 39–43.
22. Han, F.; Lin, S.; Liu, P.; Liu, X. J.; Tao, J.; Yi, C. Q.; Xu, H. Discovery of a novel series of thienopyrimidine as highly potent and selective PI3K inhibitors. *ACS Med. Chem. Lett.* **2015**, *6*, 434–438.
23. Stec, M. M.; Andrews, K. L.; Booker, S. K.; Caenepeel, S.; Freeman, D. J.; Jiang, J.; Liao, H.; McCarter, J.; Mullady, E. L.; Miguel, T. S.; Subramanian, R.; Tamayo, N.; Wang, L.; Yang, K.; Zalameda, L. P.; Zhang, N.; Hughes, P. E.; Norman, M. H. Structure–activity relationships of phosphoinositide 3-kinase (PI3K)/mammalian target of rapamycin (mTOR) dual inhibitors: investigations of various 6,5-heterocycles to improve metabolic stability. *J. Med. Chem.* **2011**, *54*, 5174–5184.

Graphical Abstract

To create your abstract, type over the instructions in the template box below.
Fonts or abstract dimensions should not be changed or altered.

Discovery of New Thienopyrimidine Derivatives as Potent and Orally Efficacious Phosphoinositide 3-Kinase Inhibitors

Leave this area blank for abstract info.

Songwen Lin [a,1], Chunyang Wang [a,1], Ming Ji [a], Deyu Wu [b], Yuanhao Lv [a], Li Sheng [c], Fangbin Han [d], Yi Dong [b], Kehui Zhang [b], Yakun Yang [c], Yan Li [c], Xiaoguang Chen [a,*], Heng Xu [a,*]

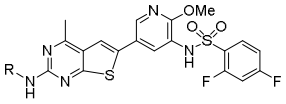

	8a R = H	**9a** R = Ac
In Vitro	IC_{50}	IC_{50}
PI3K alpha	1.3 nM	1.1 nM
NCI-H460	0.21 μM	0.062 μM
T47D	0.13 μM	0.009 μM